

***HST/STIS observations of GRB 000301C:
CCD imaging and NUV MAMA spectroscopy****

Alain Smette^{1,2,3}, Andrew S. Fruchter⁴, Theodore R. Gull¹, Kailash C. Sahu⁴, Larry Petro⁴,
Henry Ferguson⁴, James Rhoads⁴, Don J. Lindler⁵, Rachel Gibbons⁴, David W. Hogg^{6,7},
Chryssa Kouveliotou^{8,9}, Mario Livio⁴, Duccio Macchett^{4,10}, Mark R. Metzger¹¹, Holger
Pedersen¹², Elena Pian¹³, Stephen E. Thorsett^{14,15}, Ralph A.M.J. Wijers¹⁶, Johan P. U.
Fynbo^{17,18}, Javier Gorosabel¹⁹, Jens Hjorth¹², Brian L. Jensen¹², Alan Levine²⁰, Donald A.
Smith²⁰, Tom Cline¹, Kevin Hurley²¹, Jack Trombka¹

¹NASA Goddard Space Flight Center, Greenbelt MD 20771, USA;
asmette@band3.gsfc.nasa.gov, gull@sea.gsfc.nasa.gov, cline@lheavx.gsfc.nasa.gov,
uljit@lepvax.gsfc.nasa.gov

²National Optical Astronomy Observatories, P.O. Box 26732, 950 North Cherry Avenue, Tucson AZ 85726-6732, USA.

³Collaborateur Scientifique, FNRS, Belgium.

⁴Space Telescope Science Institute, 3700 San Martin Drive, Baltimore MD 21218, USA;
fruchter@stsci.edu, sahu@stsci.edu, petro@stsci.edu ferguson@stsci.edu, rhoads@stsci.edu, gibbons@stsci.edu, livio@stsci.edu, macchett@stsci.edu,

⁵Advanced Computer Concepts, Inc./Goddard Space Flight Center, Code 681, Greenbelt MD 20771, USA; lindler@rockit.gsfc.nasa.gov

⁶Institute for Advanced Study, Princeton NJ 08540, USA; hogg@ias.edu

⁷Hubble Fellow.

⁸NASA Marshall Space Flight Center, ES-84, Huntsville AL 35812, USA;
chryssa.kouveliotou@msfc.nasa.gov

⁹Universities Space Research Association.

¹⁰Affiliated to the Astrophysics Division, Space Science Department, European Space Agency.

¹¹Department of Astronomy, Caltech, MS 105-24, Pasadena CA 91125, USA; mrm@grus.caltech.edu

¹²Astronomical Observatory, University of Copenhagen, Juliane Maries Vej 30, D-2100, Copenhagen Ø, Denmark; holger@ursa.astro.ku.dk, jens@astro.ku.dk, brian_j@astro.ku.dk

¹³Istituto di Tecnologie e Studio delle Radiazioni Extraterrestri, C.N.R., Via Gobetti 101, I-40129 Bologna, Italy; pian@tesre.bo.cnr.it

¹⁴Department of Astronomy and Astrophysics, University of California, Santa Cruz CA 95064, USA; thorsett@ucolick.org

¹⁵Alfred P. Sloan Research Fellow.

¹⁶State University of New York, 452 Earth and Space Sciences Building, Stony Brook, NY 11794-3800; rwijers@ourania.ess.sunysb.edu

¹⁷Institute of Physics and Astronomy, Århus University, DK-8000 Århus C., Denmark; jfynbo@ifa.au.dk

¹⁸European Southern Observatory, D-85748, Garching bei München, Germany

¹⁹Danish Space Research Institute, Juliane Maries Vej 30 DK-2100 Copenhagen O, Denmark; jgu@dsri.dk

²⁰Massachusetts Institute of Technology, Center for Space Research, 77 Massachusetts Avenue, Cambridge MA 02139, USA; aml@space.mit.edu, dasmith@space.mit.edu

²¹University of California, Berkeley, Space Sciences Laboratory, Berkeley CA 94720-7450, USA; khurley@ssl.berkeley.edu

ABSTRACT

We present *HST*/STIS observations of the optical counterpart (OT) of the γ -ray burster GRB 000301C obtained on 2000 March 6, five days after the burst. CCD clear aperture imaging reveals a $R \simeq 21.50 \pm 0.15$ source with no apparent host galaxy. An 8000 s , $1150 < \lambda/\text{\AA} < 3300$ NUV–MAMA prism spectrum shows a flat or slightly rising continuum (in f_λ) between 2800 and 3300 \AA , with a mean flux $8.7_{-1.6}^{+0.8} \pm 2.6 \text{ } 10^{-18} \text{ ergs s}^{-1} \text{ cm}^{-2} \text{ \AA}^{-1}$, and a sharp break centered at $2797 \pm 25 \text{ \AA}$. We interpret this as the H I Lyman break at $z = 2.067 \pm 0.025$ indicating the presence of a cloud with a H I column density $\log(N_{\text{HI}} \text{ cm}^2) > 18$ on the line-of-sight to the OT. This measured redshift is conservatively a lower limit to the GRB redshift. However, as all other GRBs which have deep *HST* images appear to lie on the stellar field of a host galaxy, and as the large H I column density measured here and in later ground-based observations is unlikely on a random line-of-sight, we believe we are probably seeing absorption from H I in the host galaxy. In any case, this represents the largest direct redshift determination of a γ -ray burster to date. Our data are compatible with an OT spectrum represented by a power-law with an intrinsic index $\alpha = 1.2$ ($f_\nu \propto \nu^{-\alpha}$) and no extinction in the host galaxy or with $\alpha = 0.5$ and extinction by SMC-like dust in the OT rest-frame with $A_V = 0.15$. The large N_{HI} and the lack of a detected host are similar to the situation for damped Ly- α absorbers at $z > 2$.

Subject headings: gamma rays: bursts

1. Introduction

Gamma-ray bursts (hereafter, GRB) remain mysterious nearly 30 years after their first detection (Klebesadel, Strong, & Olson 1973), although some progress has been made in their understanding. The large sample of events collected by the BATSE experiment on-board the Compton Gamma-Ray Observatory shows an isotropic angular distribution (Meegan et al. 1992). However, their intensity distribution shows fewer weak bursts than expected from a homogeneous distributions of sources in a Euclidean space. It was therefore thought that GRBs were of extragalactic origin (Meegan et al. 1992).

* Based on observations with the NASA/ESA Hubble Space Telescope, obtained at the Space Telescope Science Institute, which is operated by the Association of Universities for Research in Astronomy, Inc. under NASA contract No. NAS5-26555.

Rapidly distributed arcminute localizations derived from X-ray instruments such as those on *BeppoSAX* (Costa et al. 1997) and, more recently, *RXTE* (Smith et al. 1999) satellites have revealed the existence of fading afterglows and enabled efficient searches for GRB counterparts to be carried out at other wavelengths. The optical transient (hereafter, OT) to GRB 970228 was the first to be discovered (van Paradijs et al. 1997). Its location angularly close to a faint diffuse object, possibly a galaxy, suggested that they are associated, providing further evidence that GRBs lie at cosmological distances (van Paradijs et al. 1997; Sahu et al. 1997, later, Fruchter et al. (1999a) showed that the diffuse object is indeed a $V = 25.8$ galaxy). This hypothesis was soon confirmed when a direct spectrum of the OT to GRB 970508 revealed absorption lines at the same redshift as the underlying $z = 0.835$ galaxy (Metzger et al. 1997; Bloom et al. 1998). Since then, OTs have been found for roughly half of the GRBs for which an X-ray afterglow has been detected and most of them appear to be associated with faint, $z > 0.4$ galaxies (Hogg & Fruchter 1999; Kulkarni et al. 2000). In particular, the probable host galaxy of GRB 971214 has a redshift of $z = 3.42$ (Kulkarni et al. 1998).

Most popular theories describing the GRB phenomenon suggest that GRB activity will be closely tied in time to episodes of massive star formation. The collapse of massive stars (Paczyński 1998) requires an active or recently active star forming host, while most neutron star – neutron star or neutron star – black hole binary mergers (Paczyński 1991; Narayan, Paczyński, & Piran 1992) occur not long after star formation. The evidence for such an environment is already suggestive, as a number of host galaxies show strong emission lines associated with star formation (Metzger et al. 1997; Djorgovski et al. 1998; Kulkarni et al. 1998; Bloom et al. 1999; Vreeswijk et al. 2000), while direct imaging with *HST/STIS* and NICMOS indicates that they are unusually blue with $V - H < 1$ whereas most galaxies in the Hubble Deep Field have $V - H > 1$ (Fruchter et al. 1999b). We thus expect that the spectra of OTs will show evidence that the events take place in environments of massive star formation: large hydrogen column density, large extinction by dust or even absorption by molecular hydrogen (Draine 2000). All lead to features in the rest-frame UV region.

We have thus embarked on a program to obtain, as targets of opportunity, *HST/STIS* near ultraviolet spectra of GRB OTs. Although Bloom et al. (1997) have suggested using grating modes of STIS for studying GRBs, we chose to use the prism as it is the most efficient available spectral element due to its low dispersion and broad spectral coverage. Combined with the near ultraviolet, photon-counting multianode microchannel array (hereafter, NUV–MAMA) detector, the prism mode provides spectral coverage over the wavelength range $1150 \lesssim \lambda/\text{\AA} \lesssim 3300$. However, its highly non-linear dispersion makes the wavelength calibration at the red end ($2800 \lesssim \lambda/\text{\AA} \lesssim 3300$) especially critical.

Here we present *HST*/STIS clear aperture CCD imaging and the first ultraviolet spectrum of a GRB optical counterpart, GRB 000301C. This burst was detected at $9^h51^m37^s$ (UTC) on 2000 March 1 by the ASM instrument aboard the *RXTE* satellite, as well as by Ulysses and NEAR (Smith et al. 2000). Its γ -ray light curve showed a common, simple shape: singly peaked, fast–rise followed by a slow decay, lasting a total of 10 seconds, which qualifies it as a short/intermediate duration burst (Jensen et al. 2000). The resulting composite localization of area ~ 50 arcmin 2 was imaged on 2000 March 3.14–3.28 (UTC), by Fynbo et al. (2000a) with the Nordic Optical Telescope (hereafter, NOT) which revealed a then $R = 20.09 \pm 0.04$, blue optical counterpart (Jensen et al. 2000).

All exposures were taken on 2000 March 6 (UTC) during a single, 5 orbit visit. The first orbit was dedicated to imaging, acquisition and calibration. Four 2000 s NUV–MAMA prism spectra were obtained during the subsequent four orbits.

2. Imaging

The field of GRB 000301C was observed using the STIS 50CCD, clear aperture mode. In this setting no filter is interposed between the CCD and the sky, and the bandpass is determined entirely by the reflectivity of the optics and the response of the CCD. Three exposures of 480 s each were taken in a diagonal dither pattern and combined using the Drizzle algorithm and associated techniques (Fruchter & Hook 1999; Fruchter et al. 1997). The drizzled output image, presented in Figure 1, has pixels of one-half the linear dimensions of the original images, or $0.^{\hspace*{-0.1cm}\prime\prime}025355 \pm 0.000035$, since the pixel scale of the CCD is $0.^{\hspace*{-0.1cm}\prime\prime}05071 \pm 0.00007$ (Malumuth & Bowers 1997).

At the position of the optical transient of GRB 000301C we find an unresolved object (FWHM $0.^{\hspace*{-0.1cm}\prime\prime}087$) whose appearance is consistent with the STIS CCD Point Spread Function (hereafter, PSF). The mean count-rate of detected photons within 20 CCD pixels (containing more than 99.6% of the flux (Leitherer et al. 2000)) from the OT image centroid is 56.0 counts s $^{-1}$ on mean 2000 March 6.22 (UTC). Assuming a power law spectrum with $\alpha = -0.8$ and a foreground Galactic extinction with $A_V = 0.16$, as determined from the dust extinction map given by Schlegel, Finkbeiner & Davis (1998), we obtain a magnitude of $R = 21.5 \pm 0.15$, where the uncertainty is dominated by the fact that the STIS CCD clear aperture mode is not completely calibrated.

Any underlying galaxy would have to have $R \gtrsim 24$, or be unusually compact for it to avoid detection in our data. We therefore believe that the apparent flattening – the decrease of the OT luminosity fading rate – of the light curve in the R –band reported by many

observers before this image was taken (cf. Garnavich et al. (2000); Halpern et al. (2000a); Bernabei et al. (2000); Rhoads & Fruchter (2001) and references therein) is not due to an underlying host galaxy. Instead, it may either be due to the jet itself (Berger et al. 2000) or to micro-lensing (Garnavich, Loeb, & Stanek 2000). The diffuse emission to the northwest of the OT is the galaxy previously identified as a possible host (Rhoads & Fruchter 2000). From our STIS image, we derived an AB magnitude 25.1 ± 0.2 in the STIS clear aperture passband. The lack of emission between the two and the good fit between the OT and the STIS PSF suggest that the OT host galaxy has not yet been detected.

3. Spectroscopy

3.1. Acquisition and reduction

In this section, we describe the acquisition and the reduction procedures which required special attention. The reduction was performed using IDL and the GSFC version of CAL-STIS (Lindler 1999).

Each TIME-TAG, 2000 s spectrum was obtained with the prism using the 2125 Å setting – so that the spectral region corresponding to wavelengths ~ 2125 Å falls onto the central region of the NUV-MAMA detector – and the $52'' \times 0.5''$ slit. After each scientific spectrum an automatic wavelength calibration exposure was taken through the narrower $52'' \times 0.05''$ slit.

We used the $R = 18.05$ star located $\sim 5.7''$ west to the OT (cf. Fig. 1) as an offset star. The offset values were determined from the 3×900 s R -band NOT image. Acquisition took place after the STIS CCD imagery and just before the NUV-MAMA prism spectroscopy. This order allowed us to obtain the CCD images independently of the success of the spectral acquisition. However, as the acquisition produces a small change in the location of the object on the detector, an additional offset has to be taken into account for the zero-point determination of the wavelength calibration (see below).

Each scientific raw dataset displays a spectrum whose spatial profile can be modeled by a Gaussian with a mean FWHM of 2.5 pixels, or $0.072''$, as expected from a point source. There is no significant variation in the count rate between the different datasets, as well as no significant variation in the count-rate during the course of an orbit.

The sum of the sky and dark backgrounds at the location of the OT spectrum was determined for each individual exposure. It was obtained by interpolation based on a fifth degree polynomial fitted independently to each column of the image, avoiding a 20 pixel

wide region centered on the object spectrum. Extraction was performed by summing up 7 rows centered on the peak of the 2-D spectrum.

Each extracted spectrum was then wavelength calibrated. This step is especially critical, so we describe it here in more detail.

The prism dispersion relation $\lambda = \lambda(X)$ gives the wavelength λ corresponding to the pixel¹ number X in the extracted spectrum. It is well modelled by a relation

$$\lambda = \sum_{i=0}^4 \frac{a_i}{(X - X_0)^i}. \quad (1)$$

Due to the strong blending of the lines especially at the red end of the spectrum, no determination of the dispersion solution (i.e., the values of each coefficient a_i) is feasible on-orbit. Instead, the values of a_i were obtained during the pre-launch, thermal vacuum testing of STIS, using an external platinum discharge lamp fed through a vacuum monochromator, the $52'' \times 0.05''$ slit and the same 2125 \AA setting as for the observations. The residuals to the fit were then measured to have an *rms* equal to 0.16 pixels.

The quantity X_0 is, in pixels, the separation along the dispersion direction of the projected location of the object on the detector from the projected location of the center of the $52'' \times 0.05''$ slit used for the determination of the dispersion solution. X_0 determines the zero-point of the wavelength calibration for each exposure and can be represented as the sum of three quantities: (1) $\Delta\phi_{\text{row}}$, the difference in pixels between the angular separations along the dispersion direction between the OT and the offset star as determined on the STIS CCD and NOT images; (2) $\Delta\chi$, the difference in pixels between the projection on the detector of the center of the slit used for the wavelength calibration relative to its location during the pre-launch calibration; (3) $\Delta\beta$, the difference in pixels between the location of the center of the slit used during the scientific exposures ($52'' \times 0.5''$) and that used for the automatic wavelength calibration after each scientific exposure ($52'' \times 0.05''$). In the following, we describe how each of these three quantities can be determined.

The acquisition process usually centers the object in the slit used for the scientific exposure. However, the nearby $R = 18.05$ bright star was considered too close to the OT and could have interfered with the normal procedure. Instead, it was used as an offset star. Consequently, the acquisition process (a) changed the spacecraft orientation so that the offset star is centered on the slit by an on-board centroid algorithm, and then (b) modified the spacecraft pointing to take into account the offsets in right ascension and declination

¹Throughout this paper, a pixel refers to a native, 1024×1024 format MAMA pixel, not a ‘high-resolution’ pixel (cf. Woodgate et al. (1998); Kimble et al. (1998)).

between the OT and the offset star as determined on the NOT image. However, the STIS image provides more accurate, but slightly different values for these offsets, so that we can determine exactly how far the object actually is from the slit center. $\Delta\phi_{\text{row}}$ represents the difference along the dispersion direction between the two offset determinations. Note that we also checked that the on-board algorithm provided a centroid location for the offset star on the acquisition image consistent, within 0.1 CCD pixel (0.2 MAMA pixel), with the one used to determine the offset between the star and the OT on the STIS CCD image.

Ideally, $\Delta\chi$ is best determined for each scientific dataset by cross-correlating its associated wavelength calibration exposure with a pre-launch wavelength calibration exposure. Unfortunately, the internal lamps were not operated during the pre-launch tests at the same current setting as during the on-board calibration, so that the shape of the lamp spectra were too different to be useful. In order to mitigate this effect, we built a template of the prism wavelength calibration lamp at the same setting as used during our observations based on G140L, G230L and G430L wavelength calibration exposures and the relevant sensitivity curves. However, even this template does not show exactly the same shape at the red end as the wavelength calibration spectrum. The value of $\Delta\chi$ was finally obtained by cross-correlating a 61-pixel long region (along the dispersion direction) of each spectrum where the dispersion is relatively large. As a check, we measured the center of the Lyman- α geo-coronal line determined by the middle position between its edges, and found that it falls within 1/6 of a pixel of the expected location. Finally, shifts due to thermal or flexure causes were measured to be between 0.02 and 0.2 pixels from orbit to orbit, and thus probably less than 0.1 pixel during an exposure.

Finally, regular on-board STIS calibrations enable us to determine $\Delta\beta$ to better than 1/20 CCD pixel, (1/10 MAMA pixel).

Consequently, a conservative (2σ) estimate of the error on the zero-point of the wavelength calibration is 0.5 MAMA pixels, or 0.23, 1.4, 5.2, 12, 22 and 29 Å at $\lambda = 1200, 1500, 2000, 2500, 3000$ and 3300 Å, respectively.

Since the dispersion is small at ~ 2900 Å (the location of the peak), the effect of the telescope and instrument line spread function (hereafter, LSF) must be taken into account to obtain a correct estimate of the count rate per pixel. We, therefore, deconvolved the observed spectrum using the Lucy-Richardson method. Unfortunately, the blending of lines in the wavelength calibration spectrum prevents its use to create a LSF. In the absence of suitable calibration frames taking into account the effect of the Point Spread Function of the telescope itself, we use a LSF based on the shape perpendicular to the dispersion of the 2-D spectrum of the flux standard star HS 2027+0651 at about 2800 Å. Ray-tracing studies indicate that this is a good approximation of the LSF along the dispersion direction (C.W.

Bowers, private communication). This star was observed in the prism mode during a STIS calibration program. The immediate consequence is that the corrected (de-convolved) mean level of the count rate is larger by about 25% between 2800 and 3300 Å compared to the un-corrected one.

Before converting the count rate to flux, we have checked the wavelength calibration of the prism spectrum of HS 2027+0651 and deconvolved it before building a new sensitivity curve. Once converted to flux, the 4 individual spectra were rebinned to a same set of wavelengths using bi-linear interpolation and averaged. The final, flux calibrated spectrum of GRB 000301C is presented in Figure 2a.

3.2. Simulations

Since Lucy-Richardson deconvolution of a low S/N spectrum actually decreases its S/N, we prefer to compare the spectrum in total observed counts per pixel in wavelength with simulated spectra. These spectra were built using an input spectrum expressed in units of flux, multiplied by the sensitivity curve, integrated over the spectral range of each pixel, and finally convolved with the LSF. The output spectrum expressed in count-rate is then multiplied by the exposure time.

In this paper, we only consider input spectra behaving as power-law of the form $f_\nu \propto \nu^{-\alpha}$, as expected for GRB afterglows (Mészáros, Rees & Papathanassiou 1994; Sari, Piran & Narayan 1998), modified to take into account the Galactic extinction towards GRB 000301C, the Lyman- α forest absorption lines, possible absorption due to H I, H₂ as well as extinction by dust located in the host galaxy.

For the Galactic extinction in the direction towards GRB 000301C, we used the value $A_V = 0.16$ as determined from the dust extinction map given by Schlegel, Finkbeiner & Davis (1998) and the analytical expression of the Galactic extinction curve given by Pei (1992). In order to model the Lyman- α forest absorption spectrum, we first noted that the likely redshift of GRB 000301C (cf. below) falls in a range ($1.5 \lesssim z \lesssim 2.3$) where the Lyman- α forest is still poorly studied. So far, the Hubble Deep Field South (HDF) quasar is the only one in that range whose absorption spectrum has been observed at resolution high enough to determine the H I column density and Doppler parameter by Voigt profile fitting. We thus used the H I absorbers listed by Savaglio et al. (1999) to estimate an absorption spectrum due to their respective Lyman series (Ly- α to Ly-12) lines. However, we discarded the lines associated with the $z = 1.942$ Lyman-limit system seen in the HDF quasar as it is a single event whose occurrence is dominated by small number statistics. Naturally, we also

eliminated the lines due to clouds whose redshift is larger than the assumed GRB redshift in the simulation.

Absorption due to H I located in the host galaxy takes into account Lyman series lines, modeled by Voigt profiles, as well as continuous absorption. The redshift of the host galaxy z , the H I column density N_{HI} and the Doppler parameter b can be easily adjusted. The modelling of possible absorption due to H₂ located in the host galaxy follows Draine (2000).

Finally, the possible extinction due to dust in the host galaxy, characterized by the rest-frame A_V extinction and the type of dust (Small Magellanic Cloud, Large Magellanic Cloud or Milky Way) also uses the expression given by Pei (1992).

3.3. Results

Figure 2a reveals a flat or slightly rising continuum spectrum (in f_λ) over the range from 2800 Å to the sensitivity limited red end of the spectrum (3300 Å). No useful constraint on the spectral slope can be derived from the spectrum alone. The mean flux is measured to be $8.7^{+0.8}_{-1.6} \pm 2.6 \text{ } 10^{-18} \text{ ergs s}^{-1} \text{ cm}^{-2} \text{ Å}^{-1}$, where the first error values come from the uncertainties in the wavelength calibration combined with the strong slope of the sensitivity curve at ~ 2900 Å; the second error value is the standard deviation of the flux calibrated error array over the relevant pixels. However, a sharp break can be seen centered at 2797 ± 25 Å(2σ). There is no significant flux recovery at the blue end of the spectrum.

3.4. Redshift of GRB 000301C

The observed break is best interpreted as the onset of continuous absorption below the H I Lyman break due to the presence of a cloud with a large neutral hydrogen column density, located at $z = 2.067 \pm 0.025$ (2σ) in the line-of-sight to the OT. From the fact that the observed flux is zero within the error bars blueward of the break, we determine that $\log(N_{\text{HI}} \text{ cm}^2) \gtrsim 18.0$. The decreased sensitivity at the blue end combined with the possible presence of other relatively high column density clouds in the Lyman- α forest does not allow us to set a higher lower limit. An upper limit $\log(N_{\text{HI}} \text{ cm}^2) \leq 23.3$ can be set from the absence of a strong feature at the expected location of the Ly- β line at ~ 3100 Å.

Our redshift determination is confirmed by the presence of weakly or marginally detected lines, compatible with Fe II, Mg II and other low-ionization species at a redshift $z = 2.0335 \pm 0.0003$ in a Keck spectrum obtained by Castro et al. (2000). More importantly, an ESO/VLT spectrum covering the wavelength range from 3600 Å to 8220 Å, was obtained by Jensen et

al. (2000). It reveals a damped Ly- α with a large, although uncertain $\log N_{\text{HI}} = 21.2 \pm 0.5$, within the range allowed by our spectrum, as well as some associated C IV, Fe II and possibly other low-ionization lines. These lines appear at $z = 2.0404 \pm 0.0008$, a significantly larger value than Castro et al. (2000) and in reasonable agreement with our value.

The value $z = 2.067 \pm 0.025$ corresponds to the largest direct redshift measurement of the OT to a GRB so far. If we assume that the H I cloud is associated with the OT host galaxy, then the above value is the redshift of the OT. We note however that it is conservatively a lower limit to the OT redshift. Indeed, if the object giving rise to the GRB is located outside of a galactic halo or, more generally, any H I cloud, all the absorption lines detected in the OT spectrum would be due to intervening systems.

Can we set an upper limit to the GRB redshift? Although the ESO/VLT spectrum extends down to 3600 Å, its low signal-to-noise ratio at the blue end cannot allow us to exclude the presence of low column density Ly- α forest lines between 3600 Å and ~ 4000 Å. This wavelength corresponds to a firm upper limit of $z = 2.3$ to the GRB redshift. This value also corresponds to the maximal redshift for which our STIS spectrum could reveal Lyman-limit systems which have $\log(N_{\text{HI}} \text{ cm}^2) > 17$. Using the number density of Lyman-limit systems seen in QSO spectra (Stengler-Larrea et al. 1995) in the relevant redshift range, we estimate that the probability of observing *no* additional Lyman-limit system over the range $2.067 < z < 2.3$ to be 0.68. This value is too small to exclude a larger redshift than $z = 2.067 \pm 0.025$. Similarly, the probability that a random line-of-sight covering the redshift range $0 < z < 2.3$ would encounter at least one damped Ly- α system is ~ 0.25 based on the number density of damped Ly- α system determined by Rao & Turnshek (2000). This value is too large to ascertain that the redshift of the high-column density system corresponds to the redshift of GRB 000301C. In other words, our *HST*/STIS spectrum and the ESO/VLT one only allow us to limit with certainty the redshift range of the OT to be $2.067 < z < 2.3$. However, we can argue in favor of the $z = 2.067 \pm 0.025$ value for the redshift of GRB 000301C. Indeed, on one hand, damped Ly- α systems are thought to be mainly caused by merging protogalactic clumps hosted by collapsed DM halos and, consequently, forming stars as the progenitors of normal present-day galaxies (Gardner et al. 1997; Haehnelt, Steinmetz & Rauch 1998, 2000). On the other hand, most OTs discovered so far are found to be associated with galaxies (Fruchter et al. 1999b), many of which show signs of significant star formation (Metzger et al. 1997; Djorgovski et al. 1998; Kulkarni et al. 1998; Fruchter et al. 1999a,b; Bloom et al. 1999; Vreeswijk et al. 2000) for which, presumably, a large reservoir of gas is available. In summary, the unusually large H I column density and the fact that most OT host galaxies found so far appear to actively form stars lead us to believe that the absorption seen in the spectrum of GRB 000301C is most likely due to the host galaxy.

3.5. Low extinction towards GRB 000301C

When combined with the contemporaneous STIS CCD imaging, the STIS spectrum also allows us to constrain the extinction taking place in the $z = 2.067$ H I cloud towards GRB 000301C. Figure 2b compares the observed total number of counts to a simulation characterized by an intrinsic power-law spectrum with index $\alpha = 0.5$, and some extinction in the host galaxy by SMC-like dust ($A_V = 0.15$). However, in the wavelength range of the STIS spectrum, such a model is indistinguishable from one defined by an intrinsic power-law spectrum with index $\alpha = 1.2$ ($f_\nu \propto \nu^{-\alpha}$) and no extinction in the host galaxy. These two models not only are able to reproduce the appearance of our spectrum without the need of any molecular hydrogen, but also conform to the slope of the optical spectrum (Halpern et al. 2000b; Feng, Wang & Wheeler 2000; Jensen et al. 2000) within its uncertainty. They also match the count-rate of the STIS CCD image, within the 15% accuracy of the IDL routine SIM_STIS (Plait, private communication), which predicts the expected count-rate for the different STIS modes based on the individual optical components. However, if a steep spectrum with $\alpha = 1.2$ is compatible with our STIS imaging and spectroscopic data alone, a more shallow one ($\alpha \simeq 1$) is favored when ground-based observations with lower uncertainties in optical band magnitudes than the STIS-derived R magnitude are taken into account (cf. Halpern et al. (2000b); Rhoads & Fruchter (2001)). Similarly, $\alpha \lesssim 1$, models with low extinction $A_V \lesssim 0.1$ ($A_V \lesssim 0.05$) due to LMC- (Milky Way-) like dust are also consistent with the STIS data alone. They predict that the 2175 Å feature (cf. e.g. Blanco, Fonti & Orosco (1996)) should be detectable and shifted to ~ 6570 Å. However, its presence seems to be ruled out by existing optical spectra and photometry (Rhoads & Fruchter 2001; Jensen et al. 2000). Therefore a model with a relatively small amount ($A_V \lesssim 0.1$) of SMC-like dust appears to best fit the full UV/optical data.

4. Discussion and conclusion

The *HST*/STIS CCD observations of GRB 000301C revealed a $R = 21.50 \pm 0.15$ source on 2000 March 6.2 (UTC) with no trace of a host galaxy. The NUV–MAMA prism spectrum presents a relatively flat spectrum (in f_λ) between 2800 and 3300 Å, with a mean flux $8.7_{-1.6}^{+0.8} \times 10^{-18}$ ergs s^{-1} cm^{-2} \AA^{-1} and a sharp break centered at 2797 ± 25 Å, interpreted as a H I Lyman break. It indicates that the OT arises in or beyond an absorber at $z = 2.067 \pm 0.025$ similar to the ones causing the high column density systems detected in QSO spectra. The redshift and the high H I column density are confirmed by the observed $\log N_{\text{HI}} = 21.2 \pm 0.5$ damped Ly- α , Fe II, C IV and other lines observed in the ESO/VLT spectrum (Jensen et al. 2000), as well as the Mg II and Fe II lines in the Keck spectrum

(Castro et al. 2000). The lack of a detected host galaxy and the large H I column density system are similar to the situation for damped Ly- α systems at $z > 2$ (e.g. Lowenthal et al. 1995; Fynbo, Moller & Warren 1999), which are thought to be mainly caused by merging protogalactic clumps hosted by collapsed DM halos and consequently probe the progenitors of normal present-day galaxies (Gardner et al. 1997; Haehnelt, Steinmetz & Rauch 1998, 2000). Combined with the fact that other OTs are often found in star forming galaxies, presumably with large H I content, this strongly suggests that $z = 2.067 \pm 0.025$ is actually the redshift of GRB 000301C. If this is the case, our spectrum as well as the ESO/VLT and the Keck ones suggest that the line-of-sight to the OT crosses the interstellar medium of its host galaxy.

Our data are compatible with no or little extinction. The absolute magnitude of the OT at the time of the discovery image, 41.5 hours after the burst, was therefore $M_R = -26.1$ for $H_0 = 65 \text{ km s}^{-1} \text{ Mpc}^{-1}$, $\Omega = 0.3$ and $\Lambda = 0.7$. The low extinction would argue against a naive interpretation that γ -ray bursts originate in a star forming region. Instead, one might imagine this favors the hypothesis that GRB 000301C results from a neutron star – neutron star or neutron star – black hole binary merger (Paczynski 1991; Narayan, Paczynski, & Piran 1992). In this case, this relatively short duration event could have taken place at a significant distance from the host galaxy some time after a significant burst of star formation. Narayan, Paczynski, & Piran (1992) predict that the median distance between a binary merger and its host galaxy is ~ 50 kpc at the time of the burst. Consequently, it is not impossible that the nearby galaxy $\sim 2''$ to the NE (Rhoads & Fruchter 2000; Kobayashi et al. 2000) is actually the host, although it is very red where as previous hosts tend to be blue in optical – infra-red colors: we derive a $R - K'$ color of 4.9 ± 0.5 based on magnitudes measured by Rhoads & Fruchter (2000) and Veillet (2000). In particular, we cannot exclude that this galaxy lies at $z \sim 2.067$ on the basis of the existing photometry. If this is the case, its H I disk must extend over at least ~ 20 kpc ($H_0 = 65 \text{ km s}^{-1} \text{ Mpc}^{-1}$, $\Omega_0 = 0.3$ and $\Lambda = 0.7$) to cover the line-of-sight of the OT. This value is similar to the separation between the line-of-sight to the QSO Q 2233+131 and the galaxy identified by Djorgovski et al. (1996) as responsible for the $z = 3.150$ damped Ly- α in its spectrum. Spectroscopy of the galaxy $\sim 2''$ to the NE of GRB 000301C is necessary to settle the issue.

However, the present data cannot exclude that the burst itself destroys dust as high-energy photons find their way out of a dense cloud (Waxman & Draine 2000). On the other hand, the time elapsed between the formation of the GRB progenitor and the GRB event itself could be long enough for the progenitor to leave regions of large extinction as is the case for core-collapse supernovae (type IIa, Ib/c), a significant fraction of which are also little affected by extinction (e.g. Schmidt et al. 1994). Finally, the low extinction could be possibly explained if the progenitor of GRB 000301C was located in a low metallicity galaxy

which has only recently started to produce stars. The host of GRB 000301C might therefore resemble the galaxies giving rise to damped Ly- α absorbers.

Note: After this paper was submitted, the direct determination of the redshift for the optical counterparts of two other GRBs have been reported with redshifts similar or larger than the one of GRB 000301C: GRB 000926 at $z = 2.066$ (Fynbo et al. 2000b) and GRB 000131 at $z = 4.50$ (Andersen et al. 2000).

This work was supported by NASA Guaranteed Time Observer funding to the STIS Science Team and is based upon observations obtained with the NASA/ESA Hubble Space Telescope, which is operated by the Association of Universities for Research in Astronomy, Inc., under NASA contract NAS 5-26555. This work was supported in part by NASA through STIS GTO funding, by STScI GO funding under NASA contract NAS 5-26555 and by the Danish Natural Research Council (SNF). KH is grateful to JPL Contract 958056 for Ulysses support, and to NAG 5 9503 for NEAR support.

REFERENCES

Andersen, M. I. et al. 2000, A&A, 364, L54

Bernabei, S., et al. 2000, GCNC 599

Berger, E. et al. 2000, ApJ, 545, 56

Blanco, A., Fonti, S., & Orofino, V. 1996, ApJ, 462, 1020

Bloom, J.S., Sigurdsson, S., Wijers, R.A.M.J., Almaini, O., Tanvir, N.R. & Johnson, R.A. 1997, MNRAS, 292, L55

Bloom, J. S., Djorgovski, S. G., Kulkarni, S. R., & Frail, D. A. 1998, ApJ, 507, L25

Bloom, J. S., et al. 1999, ApJ, 518, L1

Castro, S.M., et al. 2000, GCNC 605

Costa, E., et al. 1997, Nature, 387, 783

Djorgovski, S.G., Pahre, M.A., Bechtold, J., & Elston, R. 1996, Nature, 382, 234

Djorgovski, S. G., et al. 1998, ApJ, 508, L17

Draine, B.T., 2000, ApJ, 532, 273

Feng, M., Wang, L., & Wheeler, J. C. 2000, GCNC 607

Fitzpatrick, E. L., & Walborn, N. R. 1990, AJ, 99, 1483

Fruchter, A.S., Hook, R.N., Busko, I.C., Mutchler, M. 1997, in ‘The 1997 *HST* Calibration Workshop with a New Generation of Instruments’, Workshop held at the Space Telescope Science Institute, Baltimore, Maryland, September 22-24, 1997, S. Casertano, R. Jedrzejewski, T. Keyes, M. Stevens (eds), p518.

Fruchter, A.S., et al. 1999, ApJ, 516, 683

Fruchter, A.S., et al. 1999, ApJ, 519, L13

Fruchter, A.S., & Hook, R.N. 1999, PASP, submitted (astro-ph/9808087)

Fynbo, J.U., Moller, P., & Warren, S.J. 1999, MNRAS, 305, 849

Fynbo, J.P.U., et al., 2000a, GCNC 570

Fynbo, J.P.U., et al., 2000b, GCNC 807

Gardner, J. P., Katz, N., Hernquist, L., Weinberg, D. H. 1997, ApJ, 484, 31

Garnavich, P., Barmby, P., Jha, S., Stanek, K., 2000, GCNC 581

Garnavich, P. M., Loeb, A., & Stanek, K.Z. 2000, ApJ, 544, L11

Haehnelt, M.G., Steinmetz, M., & Rauch, M. 1998, ApJ, 495, 647

Haehnelt, M.G., Steinmetz, M., & Rauch, M. 2000, AJ, 534, 594

Halpern, J.P., et al. 2000a, GCNC 582

Halpern, J.P., et al. 2000b, GCNC 585

Hogg, D.W., & Fruchter, A.S., 1999, ApJ, 520, 54

Jensen, B.L., Fynbo J.U., Gorosabel J., et al. 2000, A&A, submitted (astro-ph/0005609)

Kimble, R., et al. 1998, ApJ, 492, L83

Klebesadel, R.W., Strong, I.B., & Olson, R.A. 1973, ApJ, 182, L85

Kobayashi, N., Goto, M., Terada, H., Tokunaga, A.T., et al. 2000, GCNC 587

Kulkarni, S.R., et al. 1998, Nature, 393, 35

Kulkarni, S.R., et al. 2000, in the Proceedings of the 5th Huntsville Gamma-Ray Burst Symposium, held in Huntsville, Alabama, USA, October 18–22, 1999, R.M. Kippen (ed), AIP, in press

Leitherer, C., et al. 2000, STIS Instrument Handbook , Version 4.1, (Baltimore: STScI)

Lindler, D. 1999, CALSTIS reference guide <http://hires.gsfc.nasa.gov/stis/software/calstis.html>

Lowenthal, J.D., Hogan, C.J., Green, R.F., Woodgate, B., Caulet, A., Brown, L. & Bechtold, J. 1995, *ApJ*, 451, 484

Malumuth, E.M., & Bowers, C.W. 1997, in ‘The 1997 *HST* Calibration Workshop with a New Generation of Instruments’, Workshop held at the Space Telescope Science Institute, Baltimore, Maryland, September 22-24, 1997, S. Casertano, R. Jedrzejewski, T. Keyes, M. Stevens (eds), p. 144

Meegan, C. A., et al. 1992, *Nature*, 355, 143

Mészáros, P., Rees, M.J., & Papanastassiou, H. 1994, *ApJ*, 432, 181

Metzger, M. R., et al. 1997, *Nature*, 387, 879

Narayan, R. , Paczyński, B., & Piran, T. 1992, *ApJ*, 395, L83

Paczyński, B. 1991, *Acta Astron.*, 41, 257

Paczyński, B. 1998, *ApJ*, 494, L45

van Paradijs, J., et al 1997, *Nature*, 386, 686

Pei, Y.C., 1992, *ApJ*, 395, 130

Rao, S.M., & Turnshek, D.A. 2000, *ApJS*, 130, 1

Rhoads, J., & Fruchter, A.S., 2000, *GCNC* 586

Rhoads, J., & Fruchter, A.S., 2001, *ApJ*, 546, 117

Sahu, K.C., et al. 1997, *Nature*, 387, 476

Sari, R., Piran, T., & Narayan, R. 1998, *ApJ*, 497, L17

Savaglio, S., et al., 1999, *ApJ*, 515, L5

Schlegel, D. J., Finkbeiner, D. P., & Davis, M. 1998, *ApJ*, 500, 525

Schmidt, B.P., et al. 1994, *ApJ*, 432, 42

Smith, D.A., et al. 1999, *ApJ*, 526, 683

Smith, D.A., et al. 2000, *GCNC* 568

Stengler-Larrea, E. A., et al. 1995, *ApJ*, 444, 64

Veillet, C. 2000, *GCNC* 592

Vreeswijk, P.M., et al. 2000, *ApJ*, submitted

Waxman, E., & Draine, B.T. 2000, *ApJ*, 537, 796

Woodgate, B.E., et al. 1998, *PASP*, 110, 1183

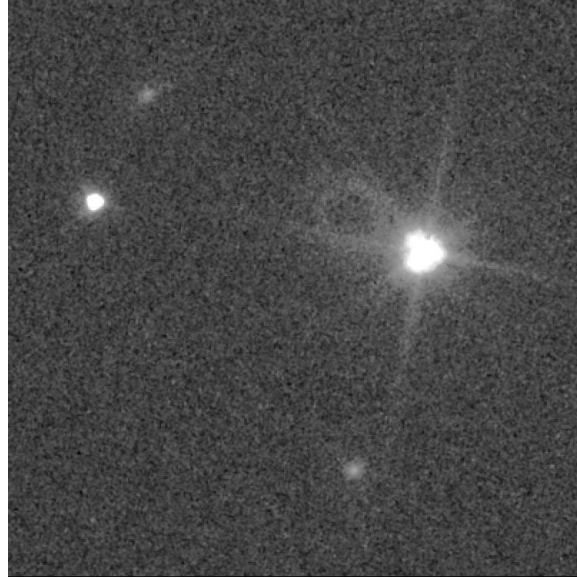


Fig. 1.— A $10'' \times 10''$ portion of the *HST*/STIS clear aperture CCD image of the field of GRB 000301C showing the OT on the left and the offset star used for acquisition on the right. North is up and East is to the left. The ring visible on the left of the offset star is a ghost due to internal reflections in the STIS CCD window.

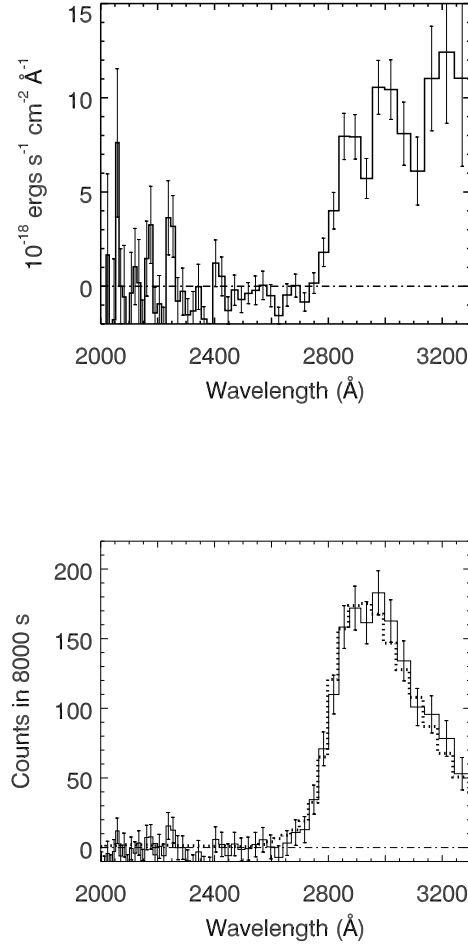


Fig. 2.— (a) *Top*: Deconvolved, flux calibrated, UV spectrum of GRB 000301C. A break is clearly seen at $\lambda 2797 \text{ \AA}$. If caused by the onset of Lyman continuous absorption due to H I gas associated with the host galaxy, the OT redshift is $z = 2.067 \pm 0.025$. (b) *Bottom*: Comparison of the observed UV spectrum, expressed in observed total number of counts with simulated spectra. The dotted curve corresponds to a model with $\alpha = 0.5$ and extinction by a SMC-like dust with $A_V = 0.15$. A model with $\alpha = 1.2$ and no extinction would present a spectrum indistinguishable in this wavelength range from the one shown here.